Journal of Modern Optics

ISSN: (Print) (Online) Journal homepage: https://www.tandfonline.com/loi/tmop20

Temperature response of all-optical XOR logic function based on different semiconductor optical amplifiers

Amer Kotb, Gopal Verma & Wei Li

To cite this article: Amer Kotb, Gopal Verma & Wei Li (2022) Temperature response of all-optical XOR logic function based on different semiconductor optical amplifiers, Journal of Modern Optics, 69:14, 769-778, DOI: 10.1080/09500340.2022.2090630

To link to this article: https://doi.org/10.1080/09500340.2022.2090630

Published online: 23 Jun 2022.

JOURNAL OF MODERN OPTICS
2022, VOL. 69, NO. 14, 769–778
https://doi.org/10.1080/09500340.2022.2090630

Taylor & Francis
Taylor & Francis Group

RESEARCH ARTICLE

Temperature response of all-optical XOR logic function based on different semiconductor optical amplifiers

Amer Kotb [a,b], Gopal Verma [a] and Wei Li [a]

[a]GPL, State Key Laboratory of Applied Optics, Changchun Institute of Optics, Fine Mechanics, and Physics, Chinese Academy of Sciences, Changchun, People's Republic of China; [b]Department of Physics, Faculty of Science, University of Fayoum, Fayoum, Egypt

ABSTRACT

A critical area of research is studying the performance of semiconductor optical amplifiers (SOAs) at high temperatures. In this paper, the performance of all-optical exclusive-OR (XOR) logic gate is investigated at high operating temperatures (T_{OP}) using different SOAs technologies such as conventional SOAs, carrier reservoir (CR)-SOAs, reflective SOAs (RSOAs), and photonic crystal (PC)-SOAs, for the first time to our knowledge. The time-dependent differential equations of SOAs, CR-SOA, RSOAs, and PC-SOAs at different operating data rates have been solved. The performance of the XOR logic gate is evaluated by calculating the quality factors and plotting the eye diagrams for each amplifier. Besides, the dependence of the key operating parameters on the T_{OP} is examined and assessed for each scheme. The results showed that the RSOAs perform better at high temperatures than other proposed SOA technologies.

ARTICLE HISTORY
Received 22 November 2021
Accepted 13 June 2022

KEYWORDS
XOR logic gate; operating temperature; semiconductor optical amplifier; quality factor

Introduction

Because of its unique characteristics such as small size, low power consumption, wide gain bandwidth, and efficient nonlinearity, the semiconductor optical amplifier (SOA) has had a significant influence in optical networks in recent years [1]. Despite these advantages, the slow dynamic response of the conventional SOA has prompted researchers to search for an alternative that can overcome the consequences of the conventional SOA and in response to the continued increase in the use of higher speeds. One of these alternatives is the carrier reservoir (CR)-SOA, which is similar in its operation to quantum dots (QDs)-SOA [1]. Because of its inherently faster gain and phase response, the CR-SOA is an alternate technology method that overcomes the response limitation of the standard SOA and allows to execute the all-optical logic operations at a higher data rate of up to 100 Gb/s [2,3]. Reflective SOA (RSOA), on the other hand, is a special type of SOA that has an anti-reflective coating on the front facet and a high reflectivity coating on the rear facet. After travelling twice through the RSOA active medium, the input signal is amplified and reflected back to the front port. The RSOA offers more advantages than a standard SOA because of its construction, such as higher optical gain and lower noise figure at low injection currents with the energy-efficient operation [1]. The RSOAs can operate at data rates of up to 120 Gb/s while still providing acceptable performance [4]. Incorporating photonic crystals (PCs) into a standard SOA, on the other hand, lets it have a faster dynamic response, making it suitable for ultra-high-speed all-optical operation up to 160 Gb/s [5]. PCs also present a low absorption loss, suppress unwanted nonlinear effects, low power consumption, and high power transmission over other nonlinear structures [5]. Accordingly, the performance of the all-optical exclusive-OR (XOR) logic gate has been studied at high operating temperatures (T_{OP}) using the proposed four schemes, i.e. SOAs, CR-SOAs, RSOAs, and PC-SOAs. For this purpose, two symmetrical (CR)-, (R)-, or (PC)-SOAs are incorporated into the Mach–Zehnder interferometer (MZI). The MZI is the most attractive interferometer in the design of the optical Boolean functions owing to its low energy requirement, low latency, high stability, and compactness [1]. The time-dependent differential equations of each scheme have been prepared and run using Adams numerical method in Wolfram Mathematica®. The performance of the XOR operation is examined and assessed by calculating the quality factors (Q-factors) and plotting the eye diagrams at different T_{OP} using the proposed four schemes. Besides, the effect of

CONTACT Amer Kotb amer@ciomp.ac.cn GPL, State Key Laboratory of Applied Optics, Changchun Institute of Optics, Fine Mechanics, and Physics, Chinese Academy of Sciences, Changchun 130033, People's Republic of China; Department of Physics, Faculty of Science, University of Fayoum, Fayoum 63514, Egypt; Wei Li weili1@ciomp.ac.cn GPL, State Key Laboratory of Applied Optics, Changchun Institute of Optics, Fine Mechanics, and Physics, Chinese Academy of Sciences, Changchun 130033, People's Republic of China

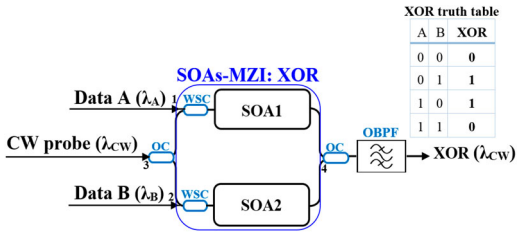

Figure 1. Schematic diagram and truth table of XOR logic gate using SOAs-MZI. CW: continuous wave. OC: 3 dB optical coupler. WSC: wavelength selective coupler. OBPF: optical bandpass filter.

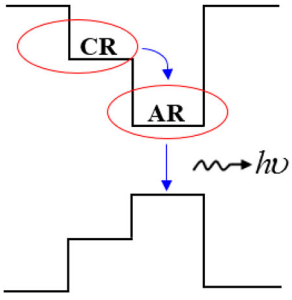

Figure 2. Band diagram of CR-SOA.

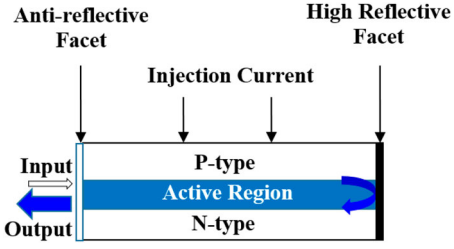

Figure 3. Schematic of RSOA.

T_{OP} on the key operating parameters is discussed for each scheme. Overall, the study concluded that the optical amplifiers should operate at low temperatures to ensure acceptable performance.

XOR gate implementation

Operation principle

InGaAsP/InP are direct band-gap semiconductor materials employed in this simulation. To realize the XOR gate using the proposed amplifiers, the operation of the RSOAs requires a circulator to enter and exit the signal from the RSOA anti-reflective front facet [4], while the other amplifiers, i.e. SOAs, QD-SOAs, and PC-SOAs, operate almost the same. Figure 1 shows the schematic diagram and truth table of the XOR logic operation utilizing ordinary SOAs-based MZI.

Two data streams A at wavelength λ_A and B at wavelength λ_B are injected via wavelength-selective couplers (WSCs) into SOA1 from port 1 and SOA2 from port 2,

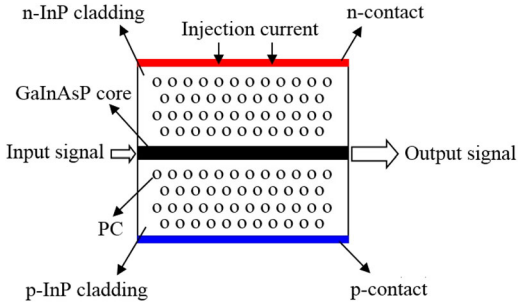

Figure 4. Schematic diagram of PC-SOA.

respectively. WSCs are typically used to combine or split many different wavelengths with low loss. A 3 dB optical coupler (OC) splits a continuous-wave (CW) probe beam into two beams, which are combined with signals A and B to inject into SOA1 and SOA2. The OC at port 3 acts as a splitter because it splits the CW input beam into two equally amplitude beams, but at output port 4 it acts as a combiner because it combines the two SOAs-MZI output signals into one XOR output signal. The CW beams interact with pulses A and B, which use cross-gain modulation and cross-phase modulation processes to induce the CW beams' gain and phase. At port 4, the CW beams interfere both constructively and destructively, resulting in varied outputs under different conditions. For example, when both A and B are '0' or '1,' the CW output beams within MZI arms have the same gain and phase, causing destructive interference at port 4, resulting in '0' output. When A is '0' and B is '1', or vice versa, the CW beams are subjected to distinct gain and phase modulations, which cause constructive interference at port 4, resulting in a '1' output. Accordingly, the XOR logic operation is functionally realized. At the CW wavelength, an optical bandpass filter (OBPF) is utilized to extract the XOR logic gate.

Modelling

Input and output signals

The return-to-zero input pulses A and B in this modelling are considered to be Gaussian-shaped pulses with energy E_0, full-wave half maximum (FWHM) pulse width τ_{FWHM}, length of the pseudorandom binary sequence (PRBS) $N = 2^7-1$ [2–5], and bit period T, which is the inverse of the operating data rate, i.e. [1–5]:

$$P_{A,B}(t) \equiv P_{in}(t) = \sum_{n=1}^{N} a_{n(A,B)} \frac{2\sqrt{\ln[2]}\,E_0}{\sqrt{\pi}\,\tau_{FWHM}} \times \exp\left[-\frac{4\ln[2](t - nT)^2}{\tau_{FWHM}^2}\right] \quad (1)$$

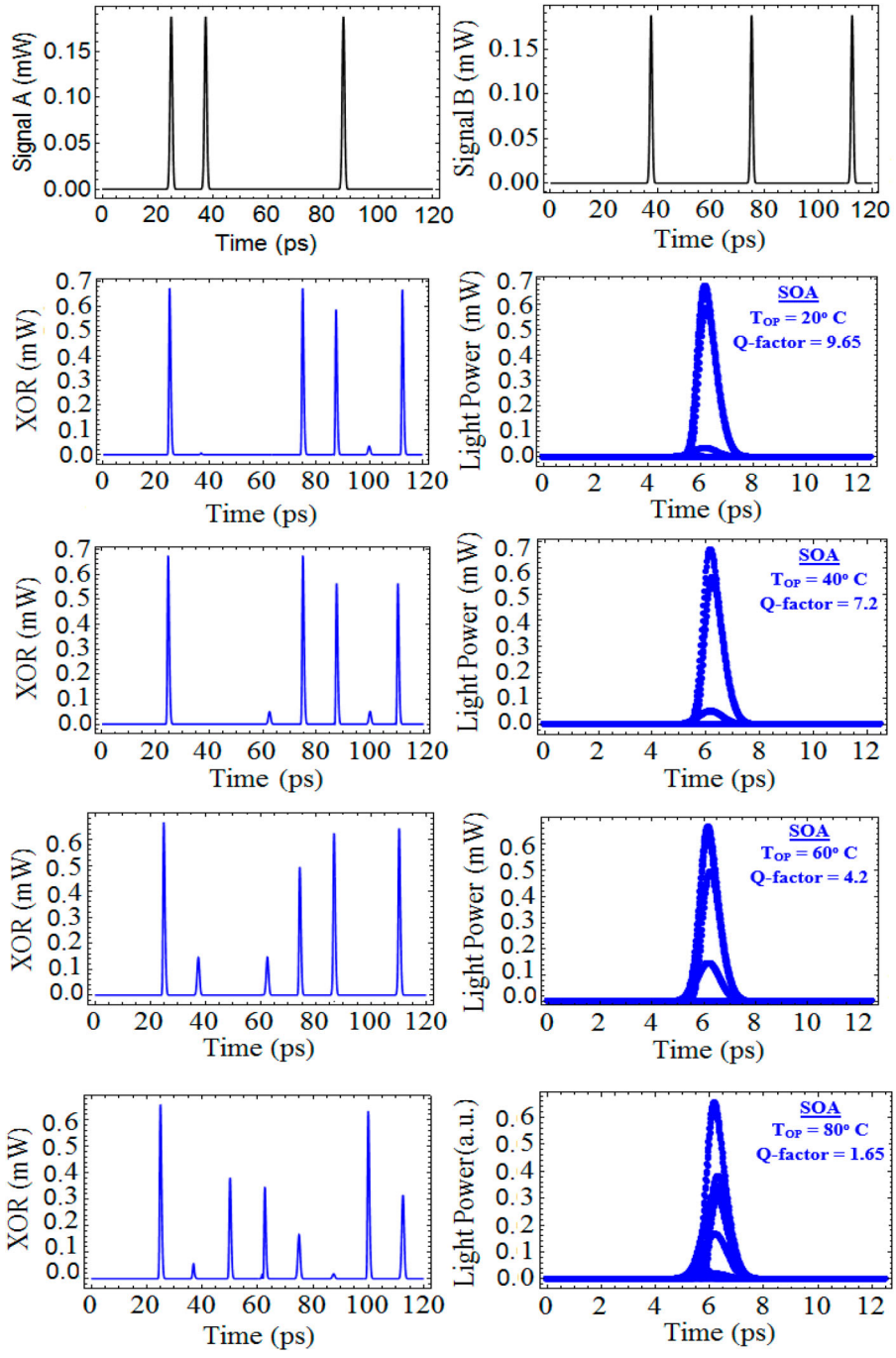

Figure 5. Pulse profiles and related eye diagram for XOR gate at different temperatures using standard SOAs-MZI at 80 Gb/s.

where $\alpha_{n(A,B)}$ denotes the binary value of the n-th bit slot in data streams A and B, i.e. $\alpha_{n(A,B)}$ = '1' or '0'. Because data A is combined with half of the CW beam in SOA1 and data B is combined with the other half of the CW beam in SOA2, the input powers in the above scheme depicted in Figure 1 are expressed as [4,5]:

$$P_{in,SOA_1}(t) = P_A(t) + 0.5P_{CW} \quad (2)$$

$$P_{in,SOA_2}(t) = P_B(t) + 0.5P_{CW} \quad (3)$$

Based on the MZI configuration, the XOR output power for all proposed schemes is then expressed by [1,2,4,5]:

$$P_{XOR}(t) = 0.25\,P_{CW}\left(G_{SOA_1}(t) + G_{SOA_2}(t) - 2\sqrt{G_{SOA_1}(t)\,G_{SOA_2}(t)}\,cos \times [\Phi_{SOA_1}(t) - \Phi_{SOA_2}(t)]\right) \quad (4)$$

Conventional SOA

For all proposed schemes, this model is taking into account the nonlinear interband effects of the carrier

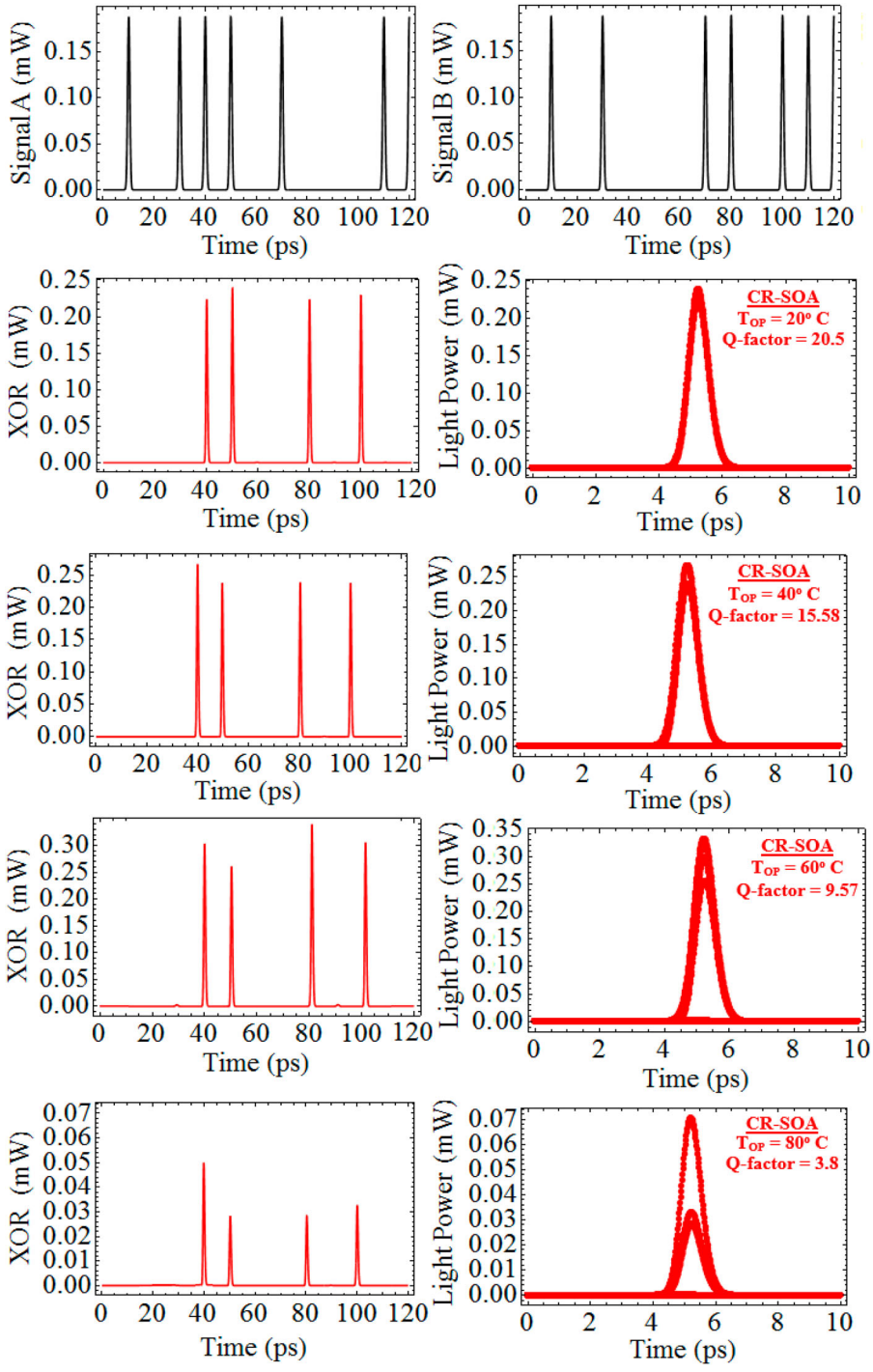

Figure 6. Pulse profiles and related eye diagram for XOR gate at different temperatures using CR-SOAs-MZI at 100 Gb/s.

depletion (CD), as well as the ultrafast intraband nonlinear effects of carrier heating (CH) and spectral hole burning (SHB). For the conventional SOAs, the time-dependent first-order coupled differential equations are given by [1]:

$$\frac{dh_{CD}(t)}{dt} = \frac{h_0 - h_{CD}(t)}{\tau_C} - (\exp[h_{CD}(t) + h_{CH}(t) + h_{SHB}(t)] - 1)\frac{P_{in}(t)}{E_{sat}} \quad (5)$$

$$\frac{dh_{CH}(t)}{dt} = -\frac{h_{CH}(t)}{\tau_{CH}} - \frac{\varepsilon_{CH}}{\tau_{CH}} - -(\exp[h_{CD}(t) + h_{CH}(t) + h_{SHB}(t)] - 1)P_{in}(t) \quad (6)$$

$$\frac{dh_{SHB}(t)}{dt} = -\frac{h_{SHB}(t)}{\tau_{SHB}} - \frac{\varepsilon_{SHB}}{\tau_{SHB}}$$

Table 1. XOR simulation default parameters using different SOAs technologies [1–9].

Symbol	Definition	Value	Unit
E_0	Pulse energy	0.7	pJ
τ_{FWHM}	Pulse width	1	ps
T	Bit period	10	ps
N	PRBS length	127	–
λ_A	Wavelength of data A	1559	nm
λ_B	Wavelength of data B	1546	nm
λ_{CW}	Wavelength of CW	1554	nm
P_{CW}	Power of CW	0.3	mW
I	Injection current	200	mA
P_{sat}	Saturation power	10	mW
τ_c	Carrier lifetime	200	ps
α	α-factor	5	–
α_{CH}	CH linewidth enhancement factor	1	–
α_{SHB}	SHB linewidth enhancement factor	0	–
ϵ_{CH}	CH nonlinear gain suppression factor	0.2	W^{-1}
ϵ_{SHB}	SHB nonlinear gain suppression factor	0.2	W^{-1}
τ_{CH}	Temperature relaxation rate	0.3	ps
τ_{SHB}	Carrier-carrier scattering rate	0.1	ps
Γ	Optical confinement factor	0.3	–
a	Differential gain	2×10^{-16}	cm^2
N_{tr}	Transparency carrier density	10^{18}	cm^{-3}
L	Length of AR	500	μm
d	Thickness of AR	0.3	μm
W	Width of AR	3	μm
G_0	Unsaturated power gain	30	dB
υ	Optical frequency	193.55	THz
B_0	Optical bandwidth	2	nm
h	Planck's constant	6.63×10^{-34}	J.s
η	Population inversion factor	0.3	–
τ_t	Transition lifetime from CR to AR	5	ps
R	Rear facet reflectivity (for RSOA)	1	–
α_{loss}	Internal loss coefficient	10	mm^{-1}
R_{loss}	Radiation loss	1500	cm^{-1}
n_g	Group index	100	–

$$\times \left(\exp\left[h_{CD}(t) + h_{CH}(t) + h_{SHB}(t)\right] - 1\right) P_{in}(t) - \frac{dh_{CD}(t)}{dt} - \frac{dh_{CH}(t)}{dt} \quad (7)$$

where h_{CD}, h_{CH}, and h_{SHB} are the gain of the SOA for the CD, CH, and SHB, respectively, integrated across the length of the SOA. E_{sat} is the saturation energy given by $E_{sat} = P_{sat}\,\tau_c = wdh\omega_0/a\Gamma$ [1], where P_{sat} is the saturation energy, τ_c is the carrier lifetime, w is the width of the active region, d is the thickness of the active region, h is the reduced Planck's constant, i.e. $h = h/2\pi$, $\omega_0 = 2\pi c/\lambda_0$ is the angular frequency, where c is the speed of light in vacuum and λ_0 is the central wavelength, a is the differential gain, and Γ is the optical confinement factor. τ_{CH} and τ_{SHB} are the temperature relaxation rates for CH and SHB, respectively. ϵ_{CH} and ϵ_{SHB} are the nonlinear gain suppression factors for CH and SHB, respectively. $h_0 = \log[G_0]$, where G_0 is the unsaturated power gain given by $G_0 = a\Gamma\,(N - N_{tr})\,L$ [1], where N is the carrier density, N_{tr} is the transparency carrier density, and L is the length of the active region. N is related to many operating parameters, including T_{OP}, through the following expression [6]:

$$N = \frac{I\tau_c}{eV} = 2\left(\frac{2\pi\, k_B\, T_{OP}}{h^2}\right)^{3/2} (m_n\, m_p)^{3/4} \times \exp\left[-\frac{E_g}{2k_B\, T_{OP}}\right] \quad (8)$$

where I is the injection current, e is the electron charge, $V = wdL$ is the volume of the active region, k_B is the Boltzmann's constant, m_n is the effective mass of the electron, m_p is the effective mass of the hole, and E_g is the energy gap. m_n and m_p are related to the electron mass (m_0) through $m_n = 0.061\, m_0$ and $m_p = 0.45\, m_0$, where $m_0 = 9.11 \times 10^{-31}$ kg [6].

The total optical gain and induced phase change, which are similar for each conventional SOA, CRSOA, and PC-SOA, are, respectively, formulated by [1–3,5]:

$$G(t) = \exp\left[h_{CD}(t) + h_{CH}(t) + h_{SHB}(t)\right] \quad (9)$$

$$\Phi(t) = -0.5\left(\alpha\, h_{CD}(t) + \alpha_{CH} h_{CH}(t) + \alpha_{SHB} h_{SHB}(t)\right) \quad (10)$$

CR-SOA

The forward injection current pushes the carriers in the CR-SOA to fill the available states in both the active region (AR) and the CR. The AR carriers are depleted by the stimulated emission process when the input optical power is present. In an ultrashort transition time of 0.5–5 ps, the carriers from the CR directly fill these depletion-uncopied AR states, as shown in Figure 2 [3]. As a result, the CR accumulates enough carriers to serve as a carrier reservoir, allowing the SOA to operate at a faster rate.

The CR-SOA time-dependent gain equations are described by the following nonlinear equations [1,3]:

$$\frac{dh_{AR}(t)}{dt} = \frac{h_{CR}(t) - h_{AR}(t)}{\tau_t(1+\eta)} + \frac{\eta h_0}{\tau_c(1+\eta)} - \frac{h_{AR}(t)}{\tau_c} - \left(\exp\left[h_{AR}(t) + h_{CH}(t) + h_{SHB}(t)\right] - 1\right)\frac{P_{in}(t)}{E_{sat}} \quad (11)$$

$$\frac{dh_{CR}(t)}{dt} = -\frac{\eta(h_{CR}(t) - h_{AR}(t)}{\tau_t(1+\eta)} + \frac{h_0 - h_{CR}(t)}{\tau_c(1+\eta)} - \frac{h_{CR}(t)}{\tau_c} \quad (12)$$

$$\frac{dh_{CH}(t)}{dt} = \frac{h_{CH}(t)}{\tau_{CH}} - \frac{\varepsilon_{CH}}{\tau CH} - \left(\exp\left[h_{AR}(t) + h_{CH}(t) + h_{SHB}(t)\right] - 1\right) P_{in}(t) \quad (13)$$

$$\frac{dh_{SHB}(t)}{dt} = -\frac{h_{SHB}(t)}{\tau_{SHB}} - \frac{\varepsilon_{SHB}}{\tau_{SHB}}$$

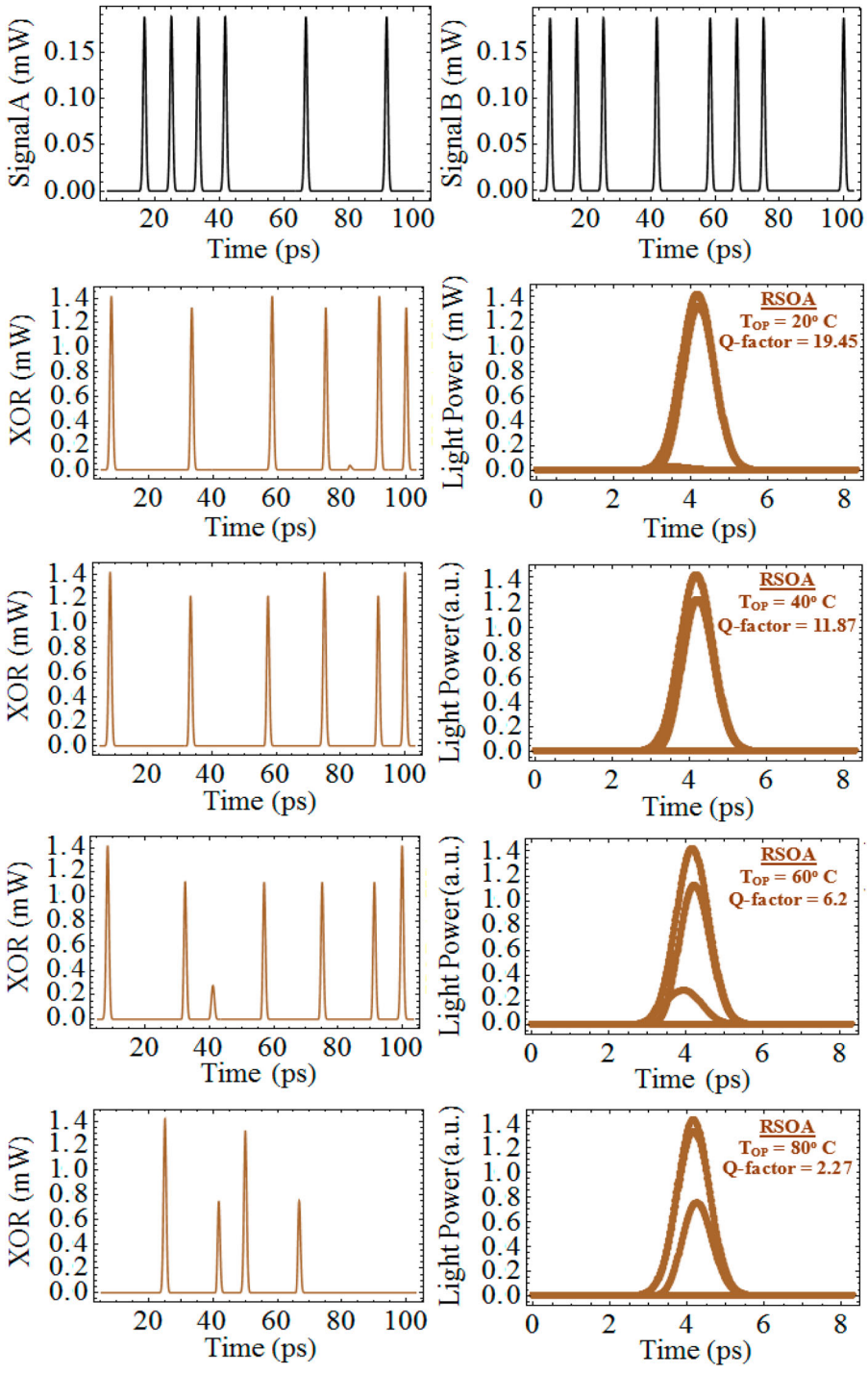

Figure 7. Pulse profiles and related eye diagram for XOR gate at different temperatures using RSOAs-MZI at 120 Gb/s.

$$\times \left(\exp\left[h_{AR}(t) + h_{CH}(t) + h_{SHB}(t)\right] - 1\right) P_{in}(t) - \frac{dh_{AR}(t)}{dt} - \frac{dh_{CH}(t)}{dt} \quad (14)$$

where h_{AR} and h_{CR} symbolize the CR-SOA gain integrated over its length for the carrier recombination between AR and CR. τ_t is the transition time from the CR layer to the AR layer and η is the population inversion factor.

RSOA

Based on the RSOA construction, the injected input light is amplified and reflected back by the rear high reflective facet to the front anti-reflective facet after passing twice through the RSOA active region as illustrated in Figure 3 [4]. This feedback process due to the forward

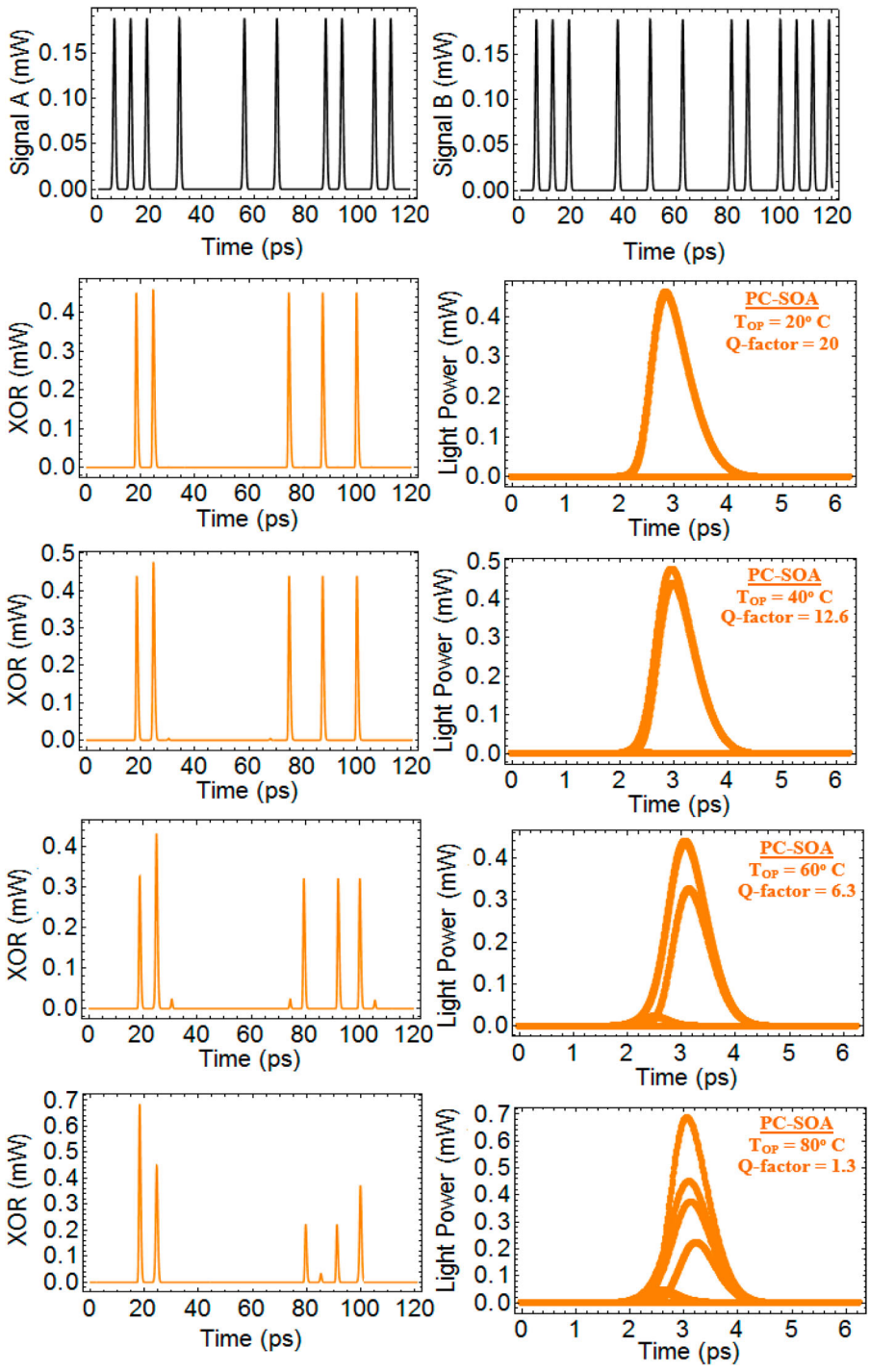

Figure 8. Pulse profiles and related eye diagram for XOR gate at different temperatures using PC-SOAs-MZI at 160 Gb/s.

and backward travelling waves in the RSOA active region saturates the gain more strongly at low input power.

The differential rate equations below characterize the time-dependent gain of each RSOA, including interband and intraband effects, i.e. [4]:

$$\frac{dh_{CD}(t)}{dt} = \frac{h_0 - h_{CD}(t)}{\tau_C} - \frac{h_{CD}(t)}{h_{CD}(t) - \alpha_{loss}L} \times (\exp[h_{CD}(t) + h_{CH}(t) + h_{SHB}(t) - \alpha_{loss}L] - 1) \times (1 + R\ \exp[h_{CD}(t) + h_{CH}(t) + h_{SHB}(t) - \alpha_{loss}L])\frac{P_{in}(t)}{E_{sat}} \quad (15)$$

$$\frac{dh_{CH}(t)}{dt} = -\frac{h_{CH}(t)}{\tau_{CH}} - \frac{\varepsilon_{CH}}{\tau_{CH}}(\exp[h_{CD}(t) + h_{CH}(t) + h_{SHB}(t) - \alpha_{loss}L] - 1)$$

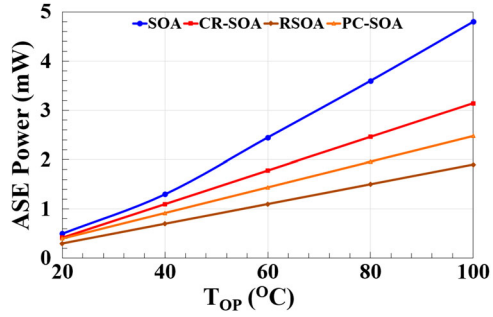

Figure 9. ASE power versus T_{OP} for conventional SOA, CR-SOA, RSOA, and PC-SOA.

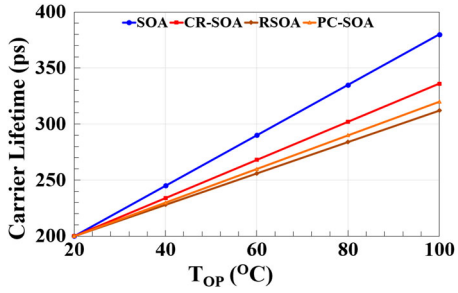

Figure 10. Carrier lifetime versus T_{OP} for conventional SOA, CR-SOA, RSOA, and PC-SOA.

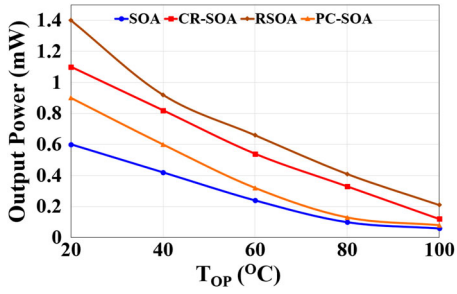

Figure 11. Output signal power versus T_{OP} for conventional SOA, CR-SOA, RSOA, and PC-SOA.

$$\times (1 + Rexp[h_{CD}(t) + h_{CH}(t) + h_{SHB}(t) - \alpha_{loss}L])\, P_{in}(t) \quad (16)$$

$$\frac{dh_{SHB}(t)}{dt} = -\frac{h_{SHB}(t)}{\tau_{SHB}} - \frac{\varepsilon_{SHB}}{\tau_{SHB}} \times (\exp[h_{CD}(t) + h_{CH}(t) + h_{SHB}(t) - \alpha_{loss}L] - 1) \times (1 + Rexp[h_{CD}(t) + h_{CH}(t) + h_{SHB}(t) - \alpha_{loss}L])\, P_{in}(t) - \frac{dh_{CD}(t)}{dt} - \frac{dh_{CH}(t)}{dt} \quad (17)$$

where α_{loss} is the internal loss coefficient and R is the rear facet reflectivity. $G_0 = \exp[2h_0]$ [4] is the unsaturated power gain with a multiplicative factor of '2' due to the twice pass of the input signal in the RSOAs active region.

For the RSOA scheme, the total optical gain and induced phase change are, respectively, expressed by [4]:

$$G(t) = R \exp[2(h_{CD}(t) + h_{CH}(t) + h_{SHB}(t) - \alpha_{loss}L)] \quad (18)$$

$$\Phi(t) = -(\alpha\, h_{CD}(t) + \alpha_{CH}\, h_{CH}(t) + \alpha_{SHB}\, h_{SHB}(t)) \quad (19)$$

PC-SOA

The holes are passing vertically and deeply through the SOA structure to form the PC-SOA, as shown in Figure 4 [5]. Reduced absorption loss, control of undesired nonlinear effects, reduced power consumption, and high power transmission are all advantages of the PC-SOA over other forms of nonlinear structures.

The time-dependent gain of each PC-SOA is described by the following differential equations [5]:

$$\frac{dh_{CD}(t)}{dt} = \frac{h_0 - h_{CD}(t)}{\tau_C} - (R_{loss}v_g)\, h_{PC}[t] - (\exp[h_{CD}(t) + h_{CH}(t) + h_{SHB}(t)] - 1)\, \frac{P_{in}(t)}{E_{sat}} \quad (20)$$

$$\frac{dh_{PC}(t)}{dt} = \left(\frac{L\,R_{loss}}{\tau_c}\right)(h_0 - h_{PC}(t)) - (R_{loss}v_g)h_{CD}(t) \quad (21)$$

$$\frac{dh_{CH}(t)}{dt} = \frac{h_{CH}(t)}{\tau_C H} - \frac{\varepsilon_{CH}}{\tau_{CH}} - (\exp[h_{CD}(t) + h_{CH}(t) + h_{SHB}(t)] - 1)\, P_{in}(t) \quad (22)$$

$$\frac{dh_{SHB}(t)}{dt} = \frac{h_{SHB}(t)}{\tau_{SHB}} - \frac{\varepsilon_{SHB}}{\tau_{SHB}} - (\exp[h_{CD}(t) + h_{CH}(t) + h_{SHB}(t)] - 1)\, P_{in}(t) - \frac{dh_{CD}(t)}{dt} - \frac{dh_{CD}(t)}{dt} \quad (23)$$

where R_{loss} is the radiation loss and v_g is the light group velocity, i.e. $v_g = c/n_g$, where n_g is the group index.

Results

Based on the default values listed in Table 1 [1–9], the aforementioned time-dependent equations for various schemes have been written and executed using Wolfram

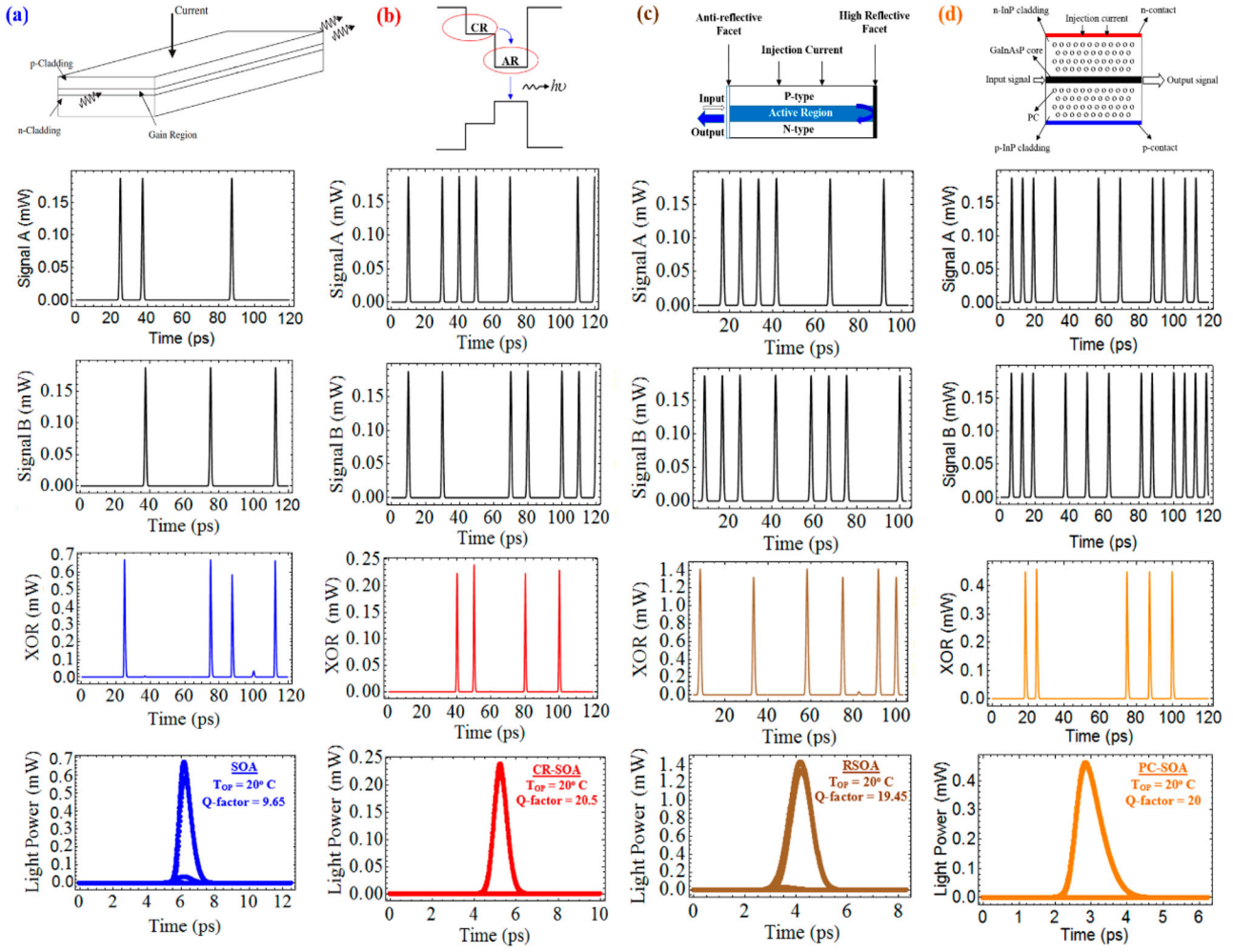

Figure 12. Performance of different SOAs-based XOR gate at $T_{OP} = 20^{o}$ C. (a) Conventional SOA, (b) CR-SOA, (c) RSOA, and (d) PC-SOA.

Mathematica's Adams numerical method. The performance of the XOR gate is evaluated by calculating the value of the Q-factor [1–5] for all schemes. A Q-factor of 6 is required for acceptable performance [1–5] to keep the corresponding bit error rate [8] below 10^{-9} [1–5].

Figures 5–8 illustrate the pulse profiles and related eye diagrams for the XOR logic function using conventional SOAs-, CR-SOAs-, RSOAs-, and PC-SOAs-based MZI at $T_{OP} = 20$, 40, 60, and 80° C, respectively. High temperatures greatly affect the performance of the proposed amplifiers, due to several reasons, (a) with a decrease in device T_{OP}, the likelihood of occupying active region energy levels increases, (b) at lower temperatures, the number of carriers available for optical gain is dispersed over a narrow range, and (c) with a drop in temperature, nonradiative recombinations decrease, causing again rise [4]. The power supply unit or the on-chip thermoelectric cooling device can both be used to manage the T_{OP}.

In the next part, we show how different critical operating parameters are affected by temperature for all the proposed amplifiers under study. We begin by studying the impact of T_{OP} on the amplified spontaneous emission (ASE) for conventional SOA, CR-SOA, RSOA, and PC-SOA as shown in Figure 9. The ASE power is expressed by $P_{ASE} = N_{SP}\ (G_0-1)\ h\upsilon B_0$ [1], where N_{sp} is the spontaneous emission factor, B_0 is the optical bandwidth, and υ is the optical frequency. This figure shows an increase of ASE power with temperature. A maximum value of 4.8 mW is observed at 100° C for the conventional SOA. The ASE does not greatly affect the performance of the RSOA because the RSOA is operated around deep saturation where the optical gain is not affected by ASE noise [4].

Figure 10 examines the effect of T_{OP} on the carrier lifetime. It is shown that an increase in T_{OP} significantly slow-down the carrier lifetime for all considered devices [10]. The ordinary SOA suffers from slow gain recovery time, which negatively affects its applications at high speeds, and the SOA situation worsens at high temperatures. The temperature of the SOA can be controlled via its power supply unit or an on-chip thermoelectric cooling unit.

For more results on the effect of T_{OP} on operating parameters, Figure 11 shows the output signal power versus T_{OP}. It is found from this figure that a significant reduction of output signal power occurs at higher temperatures owing to the reduction of the optical gain. More clarification, at low T_{OP}, the electrons available for participating in optical transitions are distributed over a narrow energy range, thus providing gain, at a given energy, becomes more. The RSOA offers a better performance as a result of the double path that the optical signal takes through its active layer.

Figure 12 presents a comparison of the pulse profiles and corresponding eye diagrams for different types of SOAs-based XOR gate at $T_{OP} = 20^{o}$ C for easy understanding and knowledge of the performance of each amplifier separately. The comparison shows the superiority of alternatives (i.e. CR-SOAs, RSOAs, and PC-SOAs) in performance over the conventional SOAs.

Conclusions

In this paper, we studied the effect of the operating temperature on the performance of the all-optical XOR logic gate using different schemes such as conventional SOAs, CR-SOAs, RSOAs, and PC-SOAs. Calculating quality factors and drawing eye diagrams at various operating temperatures are used to analyze the performance of the considered operation. In addition, for each scheme, the dependence of the major operational parameters on the operating temperature is evaluated and assessed. The results show that the conventional SOA achieves an acceptable Q-factor = 7.2 at 40^{o} C, CR-SOA achieves a much more acceptable Q-factor = 9.57 at 60^{o} C, RSOA achieves an acceptable Q-factor = 6.2 at 60^{o} C, and PC-SOA achieves an acceptable Q-factor = 6.3 at 60^{o} C. The results overall indicate that the alternatives to the conventional bulk SOA, such as CR-SOA, RSOA, and PC-SOA, can work under high temperatures, achieving an acceptable Q-factor, which is impossible for a SOA to do.

Disclosure statement

No potential conflict of interest was reported by the author(s).

Funding

Funded by Chinese Academy of Sciences President's International Fellowship Initiative (PIFI) (grant number 2022VMB 0013).

ORCID

Amer Kotb http://orcid.org/0000-0002-3776-822X
Gopal Verma http://orcid.org/0000-0003-3246-4646
Wei Li http://orcid.org/0000-0002-2227-9431

References

[1] Dutta NK, Wang Q. Semiconductor Optical Amplifiers. 2nd ed Singapore: World Scientific; 2013.
[2] Kotb A, Zoiros KE, Li W. Realization of ultrafast all-optical NAND and XNOR logic functions using carrier reservoir semiconductor optical amplifiers. J Supercomput. 2021;77:14617–14629.
[3] Kotb A, Zoiros KE, Li W. Execution of all-optical Boolean OR logic using carrier reservoir semiconductor optical amplifier-assisted delayed interferometer. Opt Laser Technol. 2021;142:107230.
[4] Kotb A, Zoiros KE, Guo C. Performance investigation of 120 Gb/s all-optical logic XOR gate using dual-reflective semiconductor optical amplifier-based scheme. J Comput Electron. 2018;17:1640–1649.
[5] Kotb A, Zoiros KE. Performance analysis of all-optical XOR gate with photonic crystal semiconductor optical amplifier-assisted Mach–Zehnder interferometer at 160 Gb/s. Opt Commun. 2017;2017(402):511–517.
[6] Khanna VK. Extreme-Temperature and Harsh-Environment Electronics: Physics, technology, and applications. Ch. 3. UK: IOP Publishing Ltd; 2017.
[7] Kotb A, Guo C. 100 Gb/s all-optical multifunctional AND, XOR, NOR, OR, XNOR, and NAND logic gates in a single compact scheme based on semiconductor optical amplifiers. Opt Laser Technol. 2021;137:106828.
[8] Thapa S, Zhang X, Dutta NK. Effects of two-photon absorption on pseudo-random bit sequence operating at high speed. J Mod Opt. 2019;66:100–108.
[9] Wang Q, Zhu G, Chen H, et al. Study of all-optical XOR using Mach–Zehnder interferometer and differential scheme. IEEE J Quantum Electron. 2004;40:703–710.
[10] Kumar Y, Shenoy MR. Enhancement in the gain recovery of a semiconductor optical amplifier by device temperature control. Pramana J Phys. 2016;87:82.